

Large Orbital Magnetic Moment in VI_3

Dávid Hovančík,* Jiří Pospíšil, Karel Carva, Vladimír Sechovský, and Cinthia Piamonteze*



Cite This: *Nano Lett.* 2023, 23, 1175–1180



Read Online

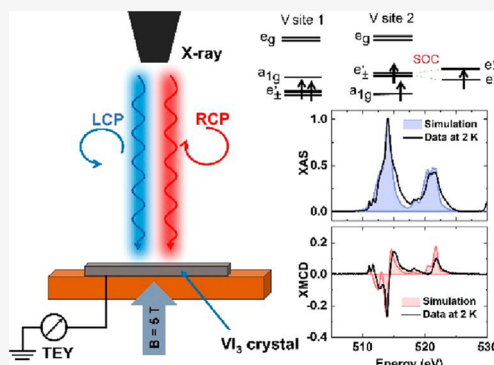
ACCESS |

Metrics & More

Article Recommendations

Supporting Information

ABSTRACT: The existence of the V^{3+} -ion orbital moment is an open issue of the nature of magnetism in the van der Waals ferromagnet VI_3 . The huge magnetocrystalline anisotropy in conjunction with the significantly reduced ordered magnetic moment compared to the spin-only value provides strong but indirect evidence of a large V orbital moment. We used the unique capability of X-ray magnetic circular dichroism to determine the orbital component of the total magnetic moment and provide a direct proof of an exceptionally sizable orbital moment of the V^{3+} ion in VI_3 . Our ligand field multiplet simulations of the XMCD spectra in synergy with the results of DFT calculations agree with the existence of two V sites with different orbital occupations and OM magnitudes in the ground state.



KEYWORDS: 2D van der Waals magnet, X-ray magnetic circular dichroism, orbital moment, VI_3

Two-dimensional (2D) van der Waals (vdW) magnetic materials have recently attracted ever-increasing interest from materials researchers because their stable magnetic ordering, even in atomically thin monolayers, provides great opportunities for spintronic devices.^{1–5} The magnetic ordering in 2D relies on magnetic anisotropy since Mermin and Wagner⁶ have shown that long-range magnetic order cannot exist in the one- or two-dimensional isotropic Heisenberg model. As proposed by Bruno,⁷ the magnetocrystalline anisotropy originates from anisotropy in the orbital moment (OM). In the extensively studied CrI_3 , the electronic configuration of the Cr^{3+} ion which experiences an octahedral crystal field is $t_{2g}^3, S = 3/2, L = 0$. The small magnetic OM value below $0.1 \mu_B$ was confirmed by XMCD measurements.⁸ As proposed by Kim et al.,⁹ the magnetic anisotropy of CrI_3 comes from the iodine p orbital spin-orbit coupling (SOC) and the p-d covalence between Cr and I, hence, being relatively small. Here we focus on a Mott insulator VI_3 , which began to be intensively investigated after the papers of Son et al.,¹⁰ Kong et al.,¹¹ and Tian et al.¹² on ferromagnetism in bulk crystals were published. The recent work of Lin et al.¹³ showing an anomalous increase of T_C for one or few monolayers of VI_3 further boosted this interest. In VI_3 the electrons in a partially filled t_{2g} level may possess an effective OM of magnitude given by the quantum number $l = 1$,¹⁴ which for the occupancy of two electrons leads to $S = 1, L = 1$ configuration. As S and L are antiparallel due to the less than half-filled V d-shell, one would expect a total magnetic moment of $1 \mu_B$, if the picture is not affected by other effects quenching the orbital moment. Early publications on VI_3 ^{10–12} showed huge disagreement on the magnitude of the out-of-plane (c^R

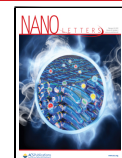
axis; c^R stands for c-axis in rhombohedral structure) magnetic moment (at 2 K and 5 T the values 2.5, 1.25, and $1.1 \mu_B/\text{V}$, respectively). Later, Liu et al. reported a moment of $1 \mu_B/\text{V}$ and proposed an unquenched OM.¹⁵ This scenario was further supported by neutron diffraction experiment done by Hao et al.,¹⁶ which found a magnetic moment of $1.2 \mu_B/\text{V}$ at 6 K. Electronic structure calculations have found a ground state where the e'_g orbital is half occupied leading to an unquenched OM.^{17,18} Strong correlations represented by Hubbard U are sufficient to open a gap between SO split bands so that this solution is semiconducting. On the other hand, another calculation suggests different semiconducting ground state with fully occupied e'_g orbitals,¹⁹ which leads to a negligible orbital moment. Direct evidence and quantification of an unquenched OM is still lacking.

TX_3 transition metal trihalides (T = transition metal, X = Cl, Br, I) adopt two common layered crystal structures with T^{3+} ions arranged in a honeycomb network at the edge-sharing octahedral coordination by six X ions (see Figure 2a). VI_3 undergoes a structural transition at 79 K between the high-temperature rhombohedral $R\bar{3}$ and low-temperature monoclinic $C2/m$ variant.^{11,20–23} Below 50 K it orders ferromagnetically with an easy-magnetization direction tilted by $\sim 40^\circ$ from

Received: October 14, 2022

Revised: January 10, 2023

Published: February 1, 2023



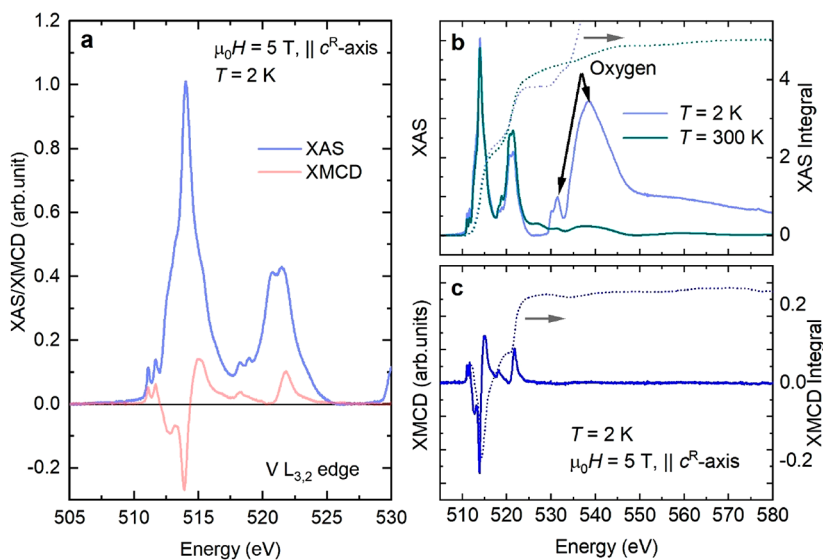


Figure 1. (a) V L_{3,2} XAS spectra of VI₃ after removing the step function and XMCD spectrum measured at 2 K. (b) XAS spectra in extended energy region and corresponding XAS integrals (dotted lines). (c) XMCD spectrum at 2 K (continuous line) and corresponding integral (dotted line).

the *c*^R-axis.^{16,24} A strong magnetic anisotropy is observed, reinforcing the proposition of an unquenched OM,²⁵ which was recently found to give rise to strong anisotropy also in FePS₃.²⁶ Around 36 K a second magnetic phase transition was proposed separating the states with one (at temperatures between 36 and 50 K) and two inequivalent magnetically ordered V sites (at lower temperatures).²⁷ In addition, a symmetry lowering from monoclinic to a triclinic structure appears at 32 K upon cooling.^{23,28} Magnetotransport measurements also show a qualitatively different ferromagnetic state below 40 K, compared to the one between *T*_c and 40 K.²⁹

Motivated by the multiple hints for nonzero OM in VI₃, we utilized the unique ability of X-ray magnetic circular dichroism (XMCD) to determine spin and orbital moments separately^{30,31} in an element-specific fashion. Our results confirm the existence of an exceptionally large OM. Ligand field multiplet simulations of the XAS and XMCD spectra are in qualitative agreement with the existence of two V sites with different orbital occupations and therefore different OM at 2 K.

Magnetization measurements show a 1.23 μ_{B} /V-ion along the easy magnetization direction, well matching the neutron-experiment result¹⁶ (see Supporting Information, Figure S1). Angular dependence of 5 T magnetization in the *ac*^R-plane at 2 K shows that the easy axis is tilted $\sim 40^\circ$ from the *c*^R-axis, also in agreement with previous publications.^{16,24,32}

Figure 1a shows the V L_{3,2} ($2p_{3/2,1/2} \rightarrow 3d$, between 505 and 530 eV) helicity-summed XAS of VI₃ and XMCD spectra derived as $\sigma^+(\omega) - \sigma^-(\omega)$ measured at 2 K and 5 T applied parallel to the *c*^R-axis. The XAS spectrum agrees well with the V³⁺ valence state published for V₂O₃ and the previous XAS published for VI₃.^{33,34} For the 2 K spectrum besides the V L_{3,2} absorption edges, we detected another two resonances above 530 eV which were identified as the O K absorption edge;³⁵ see Figure 1b. The 90 K XAS measurement (see Supporting Information, Figure S2) shows an oxygen-free spectrum (Figure 1b shows XAS spectrum taken at 300 K as reference) measured after the low-temperature data, clearly showing that the O₂ is not intrinsic to the sample surface. The likely origin

of the oxygen contribution is discussed in the Supporting Information.

From the XMCD integral shown in Figure 1c, one can notice that the value of the integrated intensity is finite and positive. According to the magneto-optical sum rules of the XMCD spectra^{30,31} (see Supporting Information, eq S1) the total integral of the XMCD signal is proportional to the OM. Therefore, the positive finite integral undoubtedly confirms the nonzero out-of-plane (*c*^R-axis) OM component antiparallel to the spin moment, as expected. Applying the magneto-optical orbital sum rules to the spectra (for $n_h = 8$, where n_h is the number of holes in the 3d orbital), we obtain $m_{\text{orb}} = 0.6 (1) \mu_{\text{B}}$. The error bar takes into account the uncertainty in determining the XAS integral due to the oxygen contribution, as detailed in the Supporting Information. The spin sum rule cannot be applied to V spectra due to the large overlap of states from the L₃ and L₂ edges, which makes the calculation of a correction factor unfeasible.^{36,37}

In VI₃ a trigonal distortion leads to a splitting of t_{2g} level into a_{1g} singlet and e_g' doublet. Two possible ground states for 3d² configurations are (i) lower energy of e_g' doublet, which would lead to the ground state with a fully occupied e_g'² level and orbital singlet with *L* = 0; (ii) electronic occupation of a_{1g}¹e_g'¹ levels where the e_g' doublet is further split by spin-orbit interaction (see Figure 2b,c,d). In the second case, the electron in the e_g' level can be assigned an effective moment analogous to p electrons with *l* = 1, and the ground state may be in the high OM state with *L* = 1.

In the case of a trigonally distorted cubic lattice, one can decide which of the two above cases is energetically favorable knowing whether the cubic body diagonal (along C₃-axis) is elongated or shortened. In VI₃ the symmetry of more distant neighbors of V beyond the octahedral I cage differs significantly from the octahedral one (see Figure 2), which may lead to corrections (of trigonal symmetry) comparable to that of the small I cage distortion. Therefore, we have employed the electronic structure DFT (for details see Supporting Information, DFT) calculations to get a more

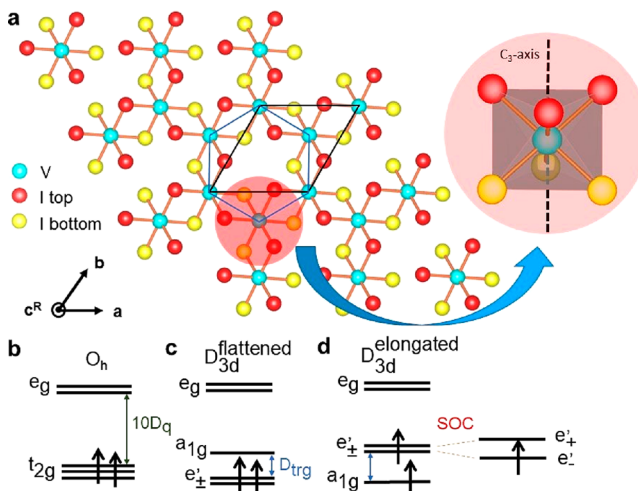


Figure 2. (a) Crystal structure of VI_3 monolayer. The VI_6 cluster is emphasized (the 3-fold axis C_3 is along the c^R -axis). (b-d) Crystal field splitting for O_h and D_{3d} (flattened/elongated octahedra) symmetry and corresponding electron occupation.

accurate picture. When both the spin-orbit interaction and correlation effects in terms of Hubbard U are included (we used $U = 4.3$ eV and Hund's exchange $J = 0.8$ eV), these calculations converge to two strikingly different solutions: either a state with quenched OM, typical for 3d transition metals, or a state with an exceptionally high OM.^{17,18} The latter state is energetically favorable, but the energy difference is small, approximately 5.6 meV according to our calculation. Under some circumstances, the state with quenched OM may become preferred; see Supporting Information, Note S1. For the spin moment, all calculations predict values close to $2 \mu_B$ in agreement with Hund rules.

For the solution with high OM, the orbital-resolved DOS for the spin-up (Figure 3 a) shows that the e'_- states are almost fully occupied while e'_+ states are empty. Notably the relevant bands are rather broad and a_{1g} character bands have a different evolution in k -space than e'_g bands. Nevertheless, one can say that a_{1g} states are generally energetically lower than e'_g as

expected for this situation. On the other hand, the solution with the quenched OM (Figure 3 b) shows for the spin-up a complete occupation of e'_- and e'_+ states whereas the a_{1g} orbital states are above the Fermi level. This solution was found previously using the VASP code with a smaller Hubbard $U = 2$ eV.¹⁹

To help understanding of the V ground state, we have also performed ligand multiplet simulation of the XAS and XMCD spectra incorporating the strong interaction between the 2p core hole and 3d electrons.³⁸ Given the broadness of some of the bands, the use of an *ab initio* electronic structure to obtain parameters for the multiplet calculation has to be done with caution. From the calculation performed without Hubbard U in order to look at single electron energy levels we estimate $E(t_{2g}) - E(e_g)$ splitting $10D_q$ to be in the range of 1.3–1.8 eV. For the multiplet simulation, we have used $10D_q = 1.5$ eV from this range. Other parameters and details of the simulation are described in the Supporting Information.

Figure 4 shows the measured spectra compared to simulations with evaluated projections of spin and orbital angular momentum into the field direction, S_z and L_z . We define quantities S_z and L_z as angular momentum divided by the reduced Planck constant \hbar . Blue curves (Figure 4a,b) correspond to a negative D_{trg} (for definition see eq S2 in Supporting Information) energy splitting which leads to e'_g orbital as the lowest in energy. This simulation corresponds to $\langle S_z \rangle = -1, \langle L_z \rangle = 0.05$ for V in the ground state at 10 K. The red simulation (Figure 4b,c), on the other hand, corresponds to a positive D_{trg} of the t_{2g} levels with a_{1g} as the lowest energy orbital giving $\langle S_z \rangle = -1, \langle L_z \rangle = 1.13$. The largest discrepancy for the simulation with e'_g is an additional positive peak at the L_2 XMCD around 520 eV. The $a_{1g}^1 e_{-1}^1$ ground state simulation shows a different intensity ratio compared to the data for the positive and negative peaks at the L_3 -edge XMCD between 513 and 515 eV. The $a_{1g}^1 e_{-1}^1$ simulation gives an unquenched OM, in qualitative agreement with the experimental finding; however, the size of m_{orb} is overestimated by a factor of 2, approximately. In the inelastic neutron scattering experiments,

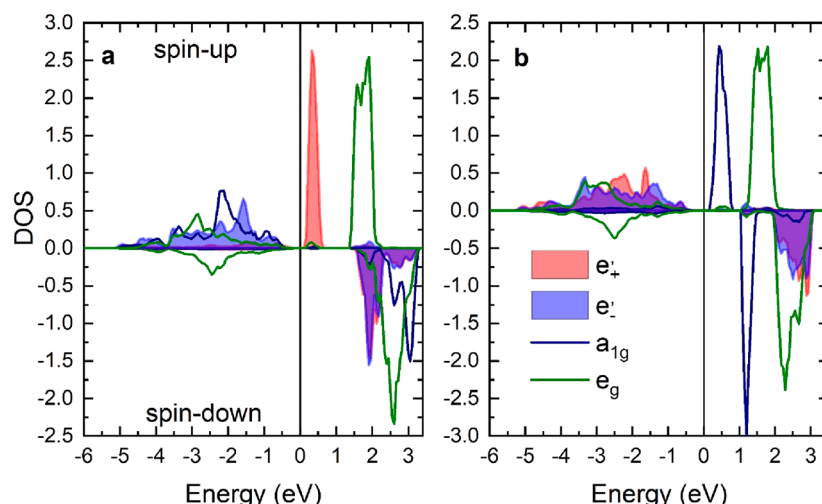


Figure 3. Calculated orbital-resolved DOS of VI_3 for spin-up/down V 3d electrons: (a) solution with high 3d OM value; (b) solutions with quenched OM. Note the violet area is the overlap of the e'_- (in blue) and e'_+ (in red) states.

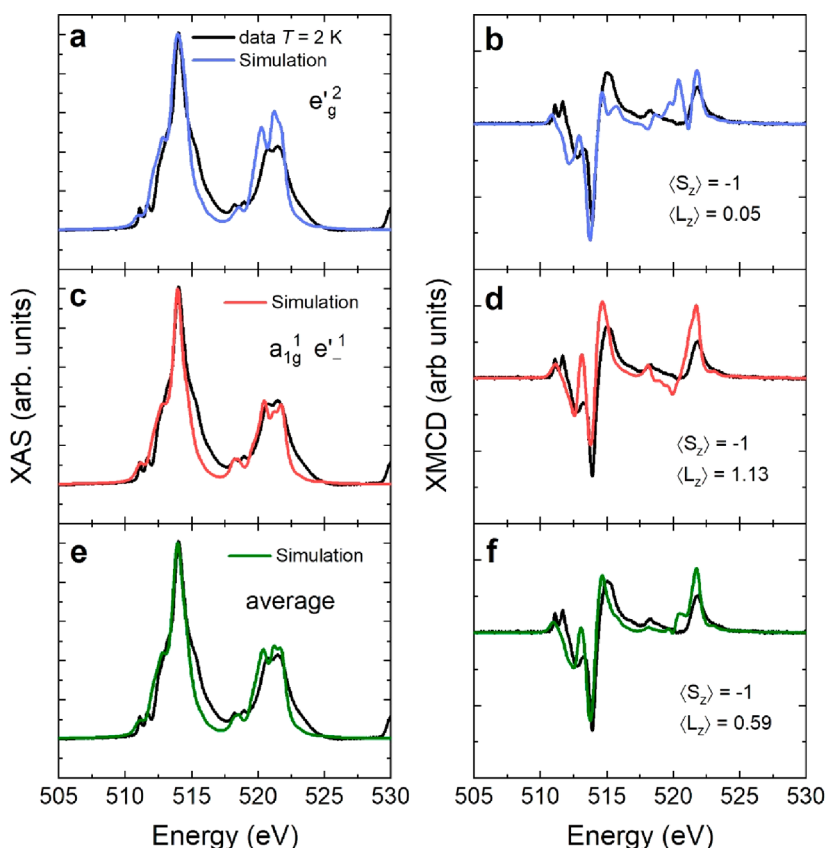


Figure 4. X-ray absorption (left panel) and X-ray magnetic circular dichroism (right panel). The data are plotted in black, while the simulations are in blue, red, and green. (a) and (b) simulations correspond to $D_{\text{trg}} = -0.15 \text{ eV}$ and a quenched OM. (c) and (d) simulations correspond to $D_{\text{trg}} = 0.3 \text{ eV}$ and an unquenched OM. (e, f) XAS and XMCD simulation is the average of (a) and (b) simulations which corresponds to an OM of $\sim 0.6 \mu_B$.

Lane et al.³⁹ have found that their observations fit only with a system composed of two simultaneously coexisting V sites with opposite trigonal distortion, where one leads to the quenched OM while the other one leads to an unquenched OM. Various kinds of coexisting different stable states for V have already been suggested in other works.^{17,27,40} The d SOC and crystal field parameters used for the simulations shown in Figure 4 are in close agreement with those used by Lane et al. To simulate the coexistence of two V sites with opposite distortions, we take the average (50% occupancy each) of the simulations for $e_g'^2$ and $a_{1g}^1 e_{-}^1$ ground state which is represented by the green curve in Figure 4e,f. The qualitative agreement between data and simulation is improved in comparison to the single site simulations. Most importantly, the average OM from the two sites, which corresponds to $0.59 \mu_B$ is in very good agreement with the value obtained from the XMCD orbital sum rule. Therefore, our results support the picture of two coexisting inequivalent V magnetic sites.

Recently an ARPES investigation has revealed a significant occupation of a_{1g} orbitals, in addition to e_g' orbitals.³⁴ In their work, the authors attribute that to V^{2+} at the surface, although their XAS agrees with V^{3+} . The argument for this proposition is based on a prediction that e_g' should be fully occupied at the ground state and only the existence of V^{2+} could then explain the observed a_{1g} occupation. The existence of a ground state with the a_{1g} orbital occupied and a high OM, as found here

following previous works,^{17,18,39} would be a reasonable explanation of the ARPES results.

The importance of many-body effects, solid-state hybridization, and the possible presence of multiple V sites in this system represent a challenging task for the theory. A more accurate spectra description may be achieved fusing advanced configuration interaction techniques or the Bethe–Salpeter equation.^{38,41}

In summary, our XMCD results unequivocally demonstrate the existence of an unquenched OM of V in VI_3 , thus resolving the long debate on this issue. Our findings are connected to theoretical models of the V ground state in VI_3 , help us to reveal which orbitals are occupied, and explain the large magnetic anisotropy observed in this system. Using ligand field multiplet simulations, we could show that the ground state of the V ion would agree with inelastic neutron scattering results where two V sites with opposite trigonal distortion were proposed.

■ ASSOCIATED CONTENT

SI Supporting Information

The Supporting Information is available free of charge at <https://pubs.acs.org/doi/10.1021/acs.nanolett.2c04045>.

Methods for crystal growth, magnetization measurements, XMCD sum rules calculation, multiplet simulations parameters, XAS/XMCD measurement conditions, and DFT calculations details ([PDF](#))

AUTHOR INFORMATION

Corresponding Authors

Dávid Hovančík – Department of Condensed Matter Physics, Faculty of Mathematics and Physics, Charles University, 121 16 Prague, Czech Republic; orcid.org/0000-0002-8931-5206; Email: hovancik@mag.mff.cuni.cz

Cinthia Piamonteze – Swiss Light Source, Paul Scherrer Institut, CH-5232 Villigen, Switzerland; orcid.org/0000-0002-8416-9668; Email: cinthia.piamonteze@psi.ch

Authors

Jiří Pospíšil – Department of Condensed Matter Physics, Faculty of Mathematics and Physics, Charles University, 121 16 Prague, Czech Republic; orcid.org/0000-0001-6642-5317

Karel Carva – Department of Condensed Matter Physics, Faculty of Mathematics and Physics, Charles University, 121 16 Prague, Czech Republic; orcid.org/0000-0002-2275-1986

Vladimír Sechovský – Department of Condensed Matter Physics, Faculty of Mathematics and Physics, Charles University, 121 16 Prague, Czech Republic; orcid.org/0000-0003-1298-2120

Complete contact information is available at:
<https://pubs.acs.org/10.1021/acs.nanolett.2c04045>

Author Contributions

D.H., C.P., and J.P. performed the XAS and XMCD measurements. The crystals were grown by J.P. D.H. measured the magnetization data. The XAS and XMCD data were analyzed by D.H. and C.P. C.P. with help of K.C. did multiplet calculations. The DFT calculations were done by K.C. V.S. wrote the manuscript with the contribution of all coauthors. All authors have approved the final version of the manuscript.

Notes

The authors declare no competing financial interest.

ACKNOWLEDGMENTS

This work is a part of Research Project GACR 21-06083S which is financed by the Czech Science Foundation. The experiments were carried out in the Materials Growth and Measurement Laboratory MGML (see <http://mgml.eu>) which is supported by the program of Czech Research Infrastructures (Project LM2018096). This project was also supported by OP VVV project MATFUN under Grant CZ.02.1.01/0.0/0.0/15_003/0000487. We thank A. Marmodoro for valuable discussions. This work was supported by the Ministry of Education, Youth and Sports of the Czech Republic through the e-INFRA CZ (Grant 90140).

REFERENCES

- (1) Duong, D. L.; Yun, S. J.; Lee, Y. H. van der Waals Layered Materials: Opportunities and Challenges. *ACS Nano* **2017**, *11*, 11803–11830.
- (2) Kumari, S.; Pradhan, D. K.; Pradhan, N. R.; Rack, P. D. Recent developments on 2D magnetic materials: challenges and opportunities. *Emergent Materials* **2021**, *4*, 827–846.
- (3) Gong, C.; Zhang, X. Two-dimensional magnetic crystals and emergent heterostructure devices. *Science* **2019**, *363*, 706.
- (4) Ahn, E. C. 2D materials for spintronic devices. *npj 2D Materials and Applications* **2020**, *4*, 17.
- (5) Miao, N.; Sun, Z. Computational design of two-dimensional magnetic materials. *WIREs Computational Molecular Science* **2022**, *12*, No. e1545.
- (6) Mermin, N. D.; Wagner, H. Absence of Ferromagnetism or Antiferromagnetism in One- or Two-Dimensional Isotropic Heisenberg Models. *Phys. Rev. Lett.* **1966**, *17*, 1133–1136.
- (7) Bruno, P. Tight-binding approach to the orbital magnetic moment and magnetocrystalline anisotropy of transition-metal monolayers. *Phys. Rev. B* **1989**, *39*, 865–868.
- (8) Frisk, A.; Duffy, L. B.; Zhang, S.; van der Laan, G.; Hesjedal, T. Magnetic X-ray spectroscopy of two-dimensional CrI₃ layers. *Mater. Lett.* **2018**, *232*, 5–7.
- (9) Kim, D.-H.; et al. Giant Magnetic Anisotropy Induced by Ligand LS Coupling in Layered Cr Compounds. *Phys. Rev. Lett.* **2019**, *122*, 207201.
- (10) Son, S.; et al. Bulk properties of the van der Waals hard ferromagnet VI₃. *Phys. Rev. B* **2019**, *99*, 041402.
- (11) Kong, T.; et al. VI₃-a New Layered Ferromagnetic Semiconductor. *Adv. Mater.* **2019**, *31*, 1808074.
- (12) Tian, S.; et al. Ferromagnetic van der Waals Crystal VI₃. *J. Am. Chem. Soc.* **2019**, *141*, 5326–5333.
- (13) Lin, Z.; et al. Magnetism and Its Structural Coupling Effects in 2D Ising Ferromagnetic Insulator VI₃. *Nano Lett.* **2021**, *21*, 9180–9186.
- (14) Khomskii, D. I. *Transition Metal Compounds*; Cambridge University Press, 2014.
- (15) Liu, Y.; Abeykoon, M.; Petrovic, C. Critical behavior and magnetocaloric effect in VI₃. *Physical Review Research* **2020**, *2*, 013013.
- (16) Hao, Y.; et al. Magnetic Order and Its Interplay with Structure Phase Transition in van der Waals Ferromagnet VI₃. *Chin. Phys. Lett.* **2021**, *38*, 096101.
- (17) Yang, K.; Fan, F.; Wang, H.; Khomskii, D. I.; Wu, H. VI₃: A two-dimensional Ising ferromagnet. *Phys. Rev. B* **2020**, *101*, 100402.
- (18) Sandratskii, L. M.; Carva, K. Interplay of spin magnetism, orbital magnetism, and atomic structure in layered van der Waals ferromagnet VI₃. *Phys. Rev. B* **2021**, *103*, 214451.
- (19) Nguyen, T. P. T.; Yamauchi, K.; Oguchi, T.; Amoroso, D.; Picozzi, S. Electric-field tuning of the magnetic properties of bilayer VI₃: A first-principles study. *Phys. Rev. B* **2021**, *104*, 014414.
- (20) Son, S.; et al. Bulk properties of the van der Waals hard ferromagnet VI₃. *Phys. Rev. B* **2019**, *99*, 041402.
- (21) Doležal, P.; et al. Crystal structures and phase transitions of the van der Waals ferromagnet VI₃. *Physical Review Materials* **2019**, *3*, 121401.
- (22) Kratochvílová, M.; et al. Crystal structure evolution in the van der Waals vanadium trihalides. *J. Phys.: Condens. Matter* **2022**, *34*, 294007.
- (23) Marchandier, T.; et al. Crystallographic and magnetic structures of the VI₃ and LiVI₃ van der Waals compounds. *Phys. Rev. B* **2021**, *104*, 014105.
- (24) Koriki, A.; et al. Magnetic anisotropy in the van der Waals ferromagnet VI₃. *Phys. Rev. B* **2021**, *103*, 174401.
- (25) Yan, J.; et al. Anisotropic magnetic entropy change in the hard ferromagnetic semiconductor VI₃. *Phys. Rev. B* **2019**, *100*, 094402.
- (26) Kim, T. Y.; Park, C.-H. Magnetic Anisotropy and Magnetic Ordering of Transition-Metal Phosphorus Trisulfides. *Nano Lett.* **2021**, *21*, 10114–10121.
- (27) Gati, E.; et al. Multiple ferromagnetic transitions and structural distortion in the van der Waals ferromagnet VI₃ at ambient and finite pressures. *Phys. Rev. B* **2019**, *100*, 094408.
- (28) Doležal, P.; et al. Crystal structures and phase transitions of the van der Waals ferromagnet VI₃. *Physical Review Materials* **2019**, *3*, 121401.
- (29) Soler-Delgado, D.; et al. Probing Magnetism in Exfoliated VI₃ Layers with Magnetotransport. *Nano Lett.* **2022**, *22*, 6149–6155.
- (30) Thole, B. T.; Carra, P.; Sette, F.; van der Laan, G. X-ray circular dichroism as a probe of orbital magnetization. *Phys. Rev. Lett.* **1992**, *68*, 1943–1946.

- (31) Carra, P.; Thole, B. T.; Altarelli, M.; Wang, X. X-ray circular dichroism and local magnetic fields. *Phys. Rev. Lett.* **1993**, *70*, 694–697.
- (32) Valenta, J.; et al. Pressure-induced large increase of Curie temperature of the van der Waals ferromagnet VI₃. *Phys. Rev. B* **2021**, *103*, 054424.
- (33) Caputo, M.; et al. Metal to insulator transition at the surface of V₂O₃ thin films: An in-situ view. *Appl. Surf. Sci.* **2022**, *574*, 151608.
- (34) De Vita, A.; et al. Influence of Orbital Character on the Ground State Electronic Properties in the van Der Waals Transition Metal Iodides VI₃ and CrI₃. *Nano Lett.* **2022**, *22*, 7034–7041.
- (35) Yang, B. X.; Kirz, J.; Sham, T. K. Oxygen K-edge absorption spectra of O₂, CO and CO₂. *Phys. Lett. A* **1985**, *110*, 301–304.
- (36) Teramura, Y.; Tanaka, A.; Jo, T. Effect of Coulomb Interaction on the X-Ray Magnetic Circular Dichroism Spin Sum Rule in 3 d Transition Elements. *J. Phys. Soc. Jpn.* **1996**, *65*, 1053–1055.
- (37) Piamonteze, C.; Miedema, P.; de Groot, F. M. F. Accuracy of the spin sum rule in XMCD for the transition-metal L edges from manganese to copper. *Phys. Rev. B* **2009**, *80*, 184410.
- (38) de Groot, F. M. F.; et al. 2p x-ray absorption spectroscopy of 3d transition metal systems. *J. Electron Spectrosc. Relat. Phenom.* **2021**, *249*, 147061.
- (39) Lane, H.; et al. Two-dimensional ferromagnetic spin-orbital excitations in honeycomb VI₃. *Phys. Rev. B* **2021**, *104*, L020411.
- (40) Huang, C.; Wu, F.; Yu, S.; Jena, P.; Kan, E. Discovery of twin orbital-order phases in ferromagnetic semiconducting VI₃ monolayer. *Phys. Chem. Chem. Phys.* **2020**, *22*, 512–517.
- (41) Dvorak, M.; Rinke, P. Dynamical configuration interaction: Quantum embedding that combines wave functions and Green's functions. *Phys. Rev. B* **2019**, *99*, 115134.

□ Recommended by ACS

Berezinskii–Kosterlitz–Thouless Transition in the Type-I Weyl Semimetal PtBi₂

Arthur Veyrat, Joseph Dufouleur, et al.

JANUARY 31, 2023
NANO LETTERS

READ ▶

Chiral Light Emission from a Hybrid Magnetic Molecule–Monolayer Transition Metal Dichalcogenide Heterostructure

Vaibhav Varade, Jana Vejpravova, et al.

JANUARY 18, 2023
ACS NANO

READ ▶

Evidence for Topological Magnon–Phonon Hybridization in a 2D Antiferromagnet down to the Monolayer Limit

Jiaming Luo, Hanyu Zhu, et al.

FEBRUARY 16, 2023
NANO LETTERS

READ ▶

Changing the Interaction of a Single-Molecule Magnetic Moment with a Superconductor

Stefan Schulte, Jörg Kröger, et al.

JANUARY 05, 2023
NANO LETTERS

READ ▶

[Get More Suggestions >](#)